CARBON letters

Original Articles
Carbon Letters Vol. 26, 31-42 (2018)

One-step microwave synthesis of magnetic biochars with sorption properties

Anton Zubrik[1,*], Marek Matik[1], Michal Lovás[1], Katarína Štefušová[1], Zuzana Danková[1], Slavomír Hredzák[1], Miroslava Václavíková[1], František Bendek[1], Jaroslav Briančin[1], Libor Machala[2], and Jiři Pechoušek[2]

[1]Institute of Geotechnics, Slovak Academy of Sciences, Kosice 04001, Slovakia
[2]Department of Experimental Physics, Faculty of Science, Palacký University, Olomouc 771 46, Czech Republic

Article Info
Received 15 October 2017
Accepted 9 February 2018

***Corresponding Author**
E-mail: zubant@saske.sk
Tel: +421-557922630

Open Access
DOI: http://dx.doi.org/10.5714/CL.2018.26.031

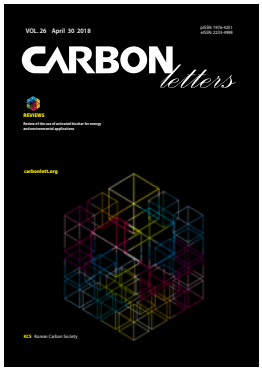

http://carbonlett.org

pISSN: 1976-4251
eISSN: 2233-4998

Abstract

Adsorption is one of the best methods for wastewater purification. The fact that water quality is continuously decreasing requires the development of novel, effective and cost available adsorbents. Herein, a simple procedure for the preparation of a magnetic adsorbent from agricultural waste biomass and ferrofluid has been introduced. Specifically, ferrofluid mixed with wheat straw was directly pyrolyzed either by microwave irradiation (900 W, 30 min) or by conventional heating (550°C, 90 min). Magnetic biochars were characterized by X-ray powder diffraction, Mössbauer spectroscopy, textural analysis and tested as adsorbents of As(V) oxyanion and cationic methylene blue, respectively. Results showed that microwave pyrolysis produced char with high adsorption capacity of As(V) (Q_m= 25.6 mg g^{-1} at pH 4), whereas conventional pyrolysis was not so effective. In comparison to conventional pyrolysis, one-step microwave pyrolysis produced a material with expressive microporosity, having a nine times higher value of specific surface area as well as total pore volume. We assumed that sorption properties are also caused by several iron-bearing composites identified by Mössbauer spectroscopy ([super] paramagnetic Fe_2O_3, α-Fe, non-stoichiometric Fe_3C, γ-Fe_2O_3, γ-Fe) transformed from nano-maghemite presented in the ferrofluid. Methylene blue was also more easily removed by magnetic biochar prepared by microwaves (Q_m=144.9 mg g^{-1} at pH 10.9) compared to using conventional techniques.

Key words: magnetic biochar, microwave pyrolysis, ferrofluid, adsorption, arsenic

1. Introduction

Water is a finite natural resource, and water pollution is one of the most pressing environmental problems that needs to be better addressed. In many regions, there is not enough water supply of appropriate quality for domestic (drinking water) or industrial use. Pollutants such as heavy metals, radionuclides, organic compounds (organic dyes, drugs, pesticides, PAHs, etc.) and other substances in water sources, even in relatively low concentration, have been identified as highly toxic and harmful to the environment and to human health. As a specific example, toxic metals/metalloids (e.g., cations of Cd, Pb, Hg, and oxyanions of As, Cr, Mo) have received increased attention due to their ability to accumulate in living organisms. Such pollutants are discharged into the environment through a number of industrial and agricultural activities.

There are several procedures for eliminating toxic substances from water. Sorption processes are considered to be promising treatment methods for the removal of metal ions in regard to cost/efficiency [1]. In recent years, considerable attention has been given to the removal of toxic metals from aqueous solutions using adsorbents derived from low-cost materials, such as agricultural waste, by-products, coal, as well as a mixture of biomass and coal [2]. Generally, adsorbents can be assumed to be low cost if they

require little processing, are abundant in nature or they are a by-product or waste material from another industry [3]. For example, pyrolysis of agricultural waste is used on a large scale to turn biomass into primary products such as bio-oil and/or gas. Secondary product biochar can be used for environmental applications (e.g., as cheap adsorbents of inorganic and/or organic pollutants) [4-12]. Biochars have also successfully been tested as cathode materials in sustainable and low-cost batteries [13]. Additionally, carbon biochars have a positive impact on soil fertility, vegetation of crops and nutrition capacity of soil, microorganism growth, cation -exchange capacity and reduction of greenhouse gases [13]. The positive soil effect relates to the textural properties as well as surface chemistry. Char produced from biomass has negatively charged sites on its porous surface, which results in the opposite charges attacking (therefore biochar is often used commercially to reduce soil acidity). In comparison to the initial biomass sample, biochar contributes a high carbon content, higher porosity and higher specific surface area. Moreover, biochar can be used as a feedstock for production of activated carbon either by chemical or physical activation in connection to a second pyrolytic step (two-stage pyrolysis) [4,14].

In general, due to their negative surface charge, biochars are effective adsorbents of toxic organic compounds and metals in cationic form. However, adsorption of metals and/or metalloids oxyanions (As, Cr) is still a demanding task. Iron-based oxides are considered to be good candidates for oxyanion removal from water [1,15]. This is due to electrostatic forces between the negatively charged arsenic and the positively charged iron oxide surface. Modification of the carbon matrix can improve the sorption properties and may lead to a higher selectivity of oxyanions. Moreover, in the case of non-magnetic sorbents (activated carbon, char), there is also a limitation connected to the solid/liquid separation [16] (it could cause the blockage of filters or the loss of carbon). Modified natural carbon materials with magnetic properties can be easily separated from water by applying an external magnetic field [17].

The synthesis of magnetic biochar is usually performed in one of three ways [18]. The first method is pyrolysis – the biomass (or other carbon material) is mixed with iron ions and then the sample is pyrolyzed. The second principle is direct modification of the biochar by iron ions through precipitation of iron ions on the carbon surface. The third technique is autoclave treatment, where agricultural waste and iron salts are treated at a defined pressure and temperature. There are also other non-conventional synthesis techniques such as mechanochemical synthesis [19] and microwave synthesis [20,21]. Recently, microwave pyrolysis has not been so frequently used for the production of pyrolytic oil or gases. However, microwave heating processes are currently subject to investigation for application in a number of fields. In contrast to conventional heating, where the material is heated from surface to core, microwaves work over the whole volume, and material is heated very quickly with quick thermal reaction. It is a homogeneous and an energetically efficient heating system [22]. In some cases, the process controlling (temperature control) is problematic, because the heating of some materials rapidly accelerates. In the case of the microwave treatment of intact biomass, where the material is heated very slowly, a susceptor of microwave irradiation (catalyzer) must be used to heat the sample (such as a carbon or a metal oxide) [23,24].

In the present work: 1) natural magnetic carbon was prepared via a one-step pyrolytic procedure (microwave and conventional pyrolysis); 2) magnetic carbon was tested as the sorbent material; or 3) magnetic susceptibility measurements showed that the material can be removed from wastewater easily using an external magnetic field/magnetic filtration.

2. Materials and Method

2.1. Preparation of magnetic carbon biochar

Magnetic biochar was prepared from agricultural waste biomass (wheat straw, WS) and ferrofluid (FF) as follows: WS (*Triticum aestivum*) was crushed (laboratory crusher FDV (MRC Ltd., Israel), and sieved to a granulometric fraction under 1 mm. Water-based FF was prepared following the patented procedure [25] by precipitation of Fe(II) and Fe(III) inorganic salts in the presence of ammonia at 80°C (water bath). Afterwards, magnetic particles were washed with deionized water to neutral pH. The magnetic nanoparticles were stabilized with oleic acid. Then, a suitable surfactant was used to disperse the particles in a carrier fluid. FF was mixed with WS (40 g of dry biomass with 200 mL of FF, ratio WS/FF=1/5) in order to produce the homogeneous magnetic paste. The fine magnetic paste was dried overnight at 80ºC, and briquettes were made and then used either for microwave or conventional pyrolysis. The elemental analysis of the

Table 1. Elemental (CHNS) analysis, ash content, total iron content and volume magnetic susceptibility (κ) of initial samples as well as samples after microwave and conventional pyrolysis

Sample	Ash[a)]	C[a)]	H[a)]	N[a)]	S[a)]	O[a)]	Fe_{Total}	κ (unit SI)
Wheat straw	7.5	43.1	6.1	0.6	0.5	45.7	-	-
WS:FF	30.1	38.3	5.6	0.4	0.7	24.9	17.4	$493{,}150 \cdot 10^{-6}$
MWpyr WS:FF	-	26.4	1.0	0.2	1.0	-	40.4	$188{,}995 \cdot 10^{-6}$
CONpyr WS:FF	-	27.9	1.1	0.4	0.9	-	34.5	$185{,}515 \cdot 10^{-6}$

Values are presented percentage.
O[a)] – by difference – according to 100 – (Ash[a)] + C[a)] + H[a)] + N[a)] + S[a)]).
[a)]Dry basis.

prepared samples is shown in Table 1.

Microwave pyrolysis was performed in a microwave oven (Panasonic NN-GD566M) with constant frequency (2450 MHz). A briquette (20 g) of the mixture WS and FF was pyrolyzed in a quartz flask at 900 W. The flask was flushed with nitrogen gas prior to the microwave conversion. After closing the vessel, the process was sustained for 30 min (obtained sample was labelled MWpyr WS:FF). Since the direct measurement of temperature is not possible during the microwave pyrolysis in a closed system, the temperature was measured by indirect method using a contactless Raytek infrared thermometer (RAYGPC series model with Marathon MM2MH sensor, temperature range 450°C–2250°C) and performed as follows: a prepared briquette of mixture WS:FF was added to the quartz flask and pyrolyzed in the microwave oven. The temperature was measured indirectly (after 10, 15, 20 min of microwave conversion), meaning the system was opened and the temperature of the sample was measured immediately with an infrared thermometer. The maximum surface temperature (950°C) was reached after 15 min.

Conventional pyrolysis of the briquette (20 g) was carried out also under nitrogen atmosphere in a horizontal quartz tube located in an electric furnace at 550ºC for 90 min (heating rate 12ºC/min). The sample was labelled as CONpyr WS:FF. After pyrolysis, both samples were washed with deionized water and also dialyzed against deionized water (10 L, 24 h).

2.2. Product analysis

CHNS analysis was performed using the elementary analyzer Vario MACRO cube (Elementar Analysensysteme GmbH, Germany) equipped with a thermal conductivity detector. The combustion tube was set to 1150ºC, and the reduction tube to 850ºC. Sulfanilamide (C=41.81%, N=16.26%, H=4.65%, S=18.62%) was used as a CHNS standard. The ash content was determined by burning in a muffle furnace at 815ºC to a constant weight. Aqua regia (a mixture of nitric acid and hydrochloric acid at a molar ratio of 1:3) was used for the dissolution of the magnetic carbon biochar to determine the total iron content by AAS (Varian 240 RS/240 Z, Australia).

Volume magnetic susceptibility (κ) was measured by Kappabridge KLY-2 apparatus (Geophysics, Czech Republic) at the following condition: magnetic field intensity 300 A m^{-1}, field homogeneity 0.2 % and frequency 920 Hz.

An X-ray powder diffraction study was carried out using a D8 Advance diffractometer (Bruker, Germany), working with Cu Kα radiation.

Surface properties of the studied samples were determined from the adsorption and desorption isotherms measured with the NOVA 1200e Surface Area & Pore Size Analyzer (Quantachrome Instruments, USA) by the method of physical adsorption of nitrogen at –196ºC. Prior to the measurements, the samples were degassed at 100ºC in a vacuum oven at a pressure below 2 Pa for 16 h. The measured data were processed by the BET (Brunauer–Emmett–Teller) isotherm [26] in the range of relative pressure 0.05–0.3 to obtain the value of specific surface area (S_A). The values of the external surface (S_{ext}) and the volume of micropores (V_{micro}) were calculated from the t-plot using the Harkins–Jura standard isotherm. The value of the total pore volume (V_{tot}) was estimated from the maximum adsorption at relative pressure close to saturation pressure. Pore size distribution was obtained from the desorption isotherm using the Barrett–Joyner–Halenda method [27].

^{57}Fe Mössbauer spectra were recorded with 512 channels and measured at room and low temperatures employing a laboratory Mössbauer spectrometer operating at a constant acceleration mode and equipped with a ^{57}Co(Rh) source. The low temperature Mössbauer spectra were recorded at 70 K and 5 K employing a Cryostation (Montana Instruments) closed-cycle cryogen-free system to which a Mössbauer spectrometer was mounted. The acquired Mössbauer spectra were processed (i.e., noise filtering and fitting) using the MossWinn software program. The isomer shift values were referred to an α-Fe foil sample at room temperature.

The particle morphology was studied by field emission scanning electron microscope, using a TESCAN MIRA3 FE (TESCAN, Czech Republic) and a high resolution transmission electron microscopy (HR-TEM) using a JEOL JEM-2100F UHR (JEOL, Japan). Prior to the TEM investigations, powders were crushed in a mortar, dispersed in ethanol and fixed on a copper-supported carbon grid.

2.3. Zeta potential

Zeta potential was measured using a Zetasizer Nano ZS (Malvern Panalytical, UK) to obtain the isoelectric point (IEP). The Zetasizer Nano measures the electrophoretic mobility of the particles, which is converted to the zeta potential using the Helmholtz–Smoluchowski equation built into the Zetasizer software. The zeta potential of the samples (concentration 2 g L^{-1}) was measured in 0.1 M $NaNO_3$ within different pH ranges, which were adjusted by the addition of 2 M NaOH or HNO_3. Afterwards, the measurements were repeated three times for each sample.

2.4. Sorption experiments

Sorption properties of magnetic chars after conventional or microwave pyrolysis were studied in reference to As(V) and methylene blue (MB). The sorption properties were studied under batch-type conditions. The sorbent concentration was 2 g L^{-1}, and the experiments were performed at room temperature in a rotary shaker set at 30 rpm with the equilibrium time of 24 h. Model solutions of As(V) were prepared by dissolving $AsHNa_2O_4 \cdot 7H_2O$ in deionized water. The metal quantity (As, Fe) in the solutions was determined by AAS. The measurement of MB concentrations was performed using a UV-VIS spectrophotometer (Helios Gamma, Thermo Electron Corporation, UK). The maximum wavelength for MB was found to be 663 nm. After adsorption, the respective concentrations were calculated using calibration curves within the range of 0–20 mg/L. The pH was adjusted by the addition of 2 M NaOH or HNO_3.

The sorption experiments were evaluated by Langmuir [28] (an isotherm for monolayer adsorption on a homogeneous surface) and Freundlich modeling [29] (an isotherm for multilayer adsorption on a heterogeneous surface), respectively. Thus, the adsorption process was well described by constants obtained

from applying both models.

The Langmuir isotherm is defined according to the equation:

$$q_e = Q_m \frac{bC_e}{1+bC_e} \quad (1)$$

where q_e is an equilibrium adsorption capacity (mg g^{-1}), Q_m is the maximum adsorption capacity (mg g^{-1}), C_e is the equilibrium metal concentration, and b is a Langmuir constant characterizing the affinity between the adsorbed molecule and the adsorbent (L mg^{-1}).

The Freundlich isotherm is defined according to:

$$q_e = K_F C_e^{\frac{1}{n}} \quad (2)$$

where K_F (L g^{-1}) and n are the constants of the isotherm.

Q_m, b, K_F and n were determined from the experimental values using the linearized form of previous equations.

In the case of the Langmuir isotherm, the linearized form is:

$$\frac{C_e}{q_e} = \frac{C_e}{Q_m} + \frac{1}{Q_m b} \quad (3)$$

The most important value is the slope ($1/Q_m$). It is the inverse value of the maximum adsorption capacity.

The linearized form of the Freundlich isotherm is as follows:

$$\ln q_e = \ln K_F + \frac{1}{n} \ln C_e \quad (4)$$

3. Results

3.1. Elemental analysis, X-ray powder diffraction and Mössbauer spectroscopy

Agricultural waste biomass (WS) contained 43.1% elemental carbon and 6.1% hydrogen (Table 1). Before the mixing of the WS with FF, the FF was studied in detail in order to know the particular phase composition. In general, FF is a colloidal suspension of magnetite or maghemite. Fig. 1a shows the X-ray diffraction patterns and Mössbauer spectroscopy study of dried FF. Several broad peaks were recorded by X-ray diffraction, which can be assigned to the spinel structure of magnetite or maghemite. X-ray diffraction is not able to differentiate between them, especially when the particles are extremely small (several nanometers) and the recorded peaks are relatively broad. Therefore, Mössbauer spectroscopy was applied in order to discern between magnetite/maghemite phases (Fig. 1b-d, Table 2). Additionally, Mössbauer spectra were taken at three different temperatures (T=5 K, T=150 K and room temperature, respectively). The room temperature Mössbauer spectrum (Figure 1B) shows a sextet with broad spectral lines, which were fitted by a distribution of hyperfine magnetic fields. An isomer shift of 0.34 mm s^{-1} and quadrupole splitting close to zero are typical for Fe^{3+} atoms with cubic symmetry in the spinel structure. More detailed information can be obtained from the low temperature Mössbauer spectra (150 K, Fig. 1c; 5 K, Fig. 1d). Both spectra were evaluated by two sextet components (Table 2) corresponding to tetrahedral and octahedral Fe atoms in the cubic spinel structure of maghemite. The ratios of the subspectrum areas slightly differ from those for stoichiometric maghemite, i.e. Tetrahedral/Octahedral=37.5%/62.5%.

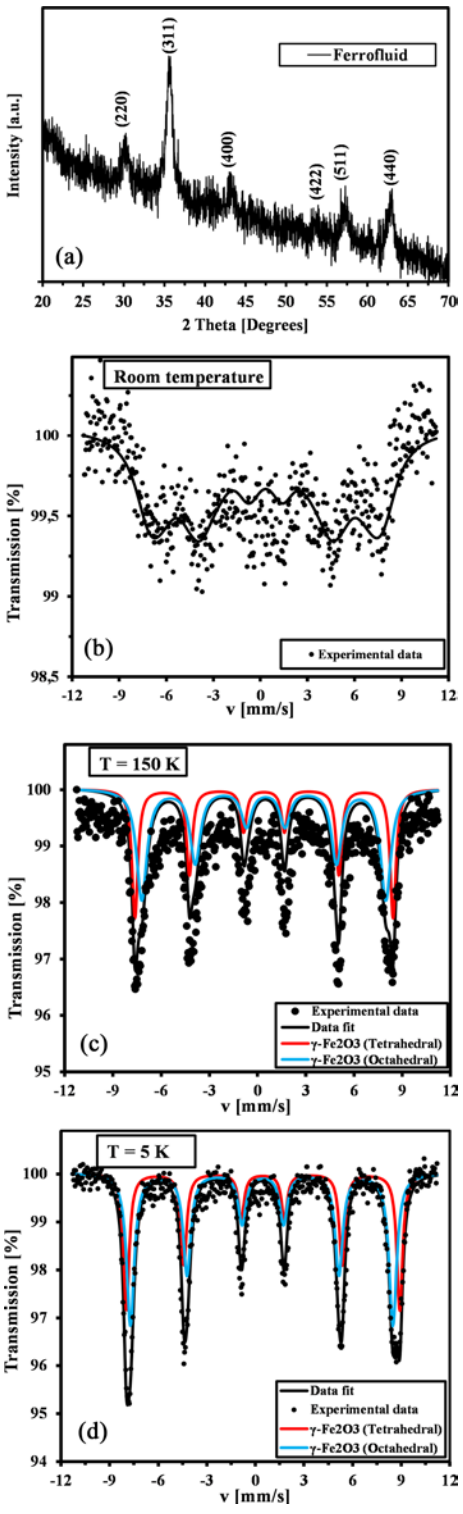

Fig. 1. X-ray powder diffraction (a) and ^{57}Fe Mössbauer spectroscopy study (b, c) of dried ferrofluid. ^{57}Fe Mössbauer spectra were taken at room temperature (b), 150 K (d) and 5 K (d), respectively.

Table 2. Mössbauer parameters for dried ferrofluid and magnetic biochar after microwave pyrolysis (MWpyr WS:FF)

Sample	IS (mm s^{-1})	QS (mm s^{-1})	H (T)	*I* (%)	Component
Ferrofluid (T=150 K)	0.40	–0.00	49.9	39.5	γ-Fe_2O_3 - sextet (tetrahedral position of Fe^{3+})
	0.45	–0.12	47.1	60.5	γ-Fe_2O_3 - sextet (octahedral position of Fe^{3+})
Ferrofluid (T=5 K)	0.47	0.01	52.4	40.4	γ-Fe_2O_3 - sextet (tetrahedral position of Fe^{3+})
	0.42	–0.07	50.3	59.6	γ-Fe_2O_3 - sextet (octahedral position of Fe^{3+})
MWpyr WS:FF	0.31	0.85	-	33.5	(Super) paramagnetic Fe_2O_3 - doublet
(room temperature)	0.00	0.00	33.2	14.3	α-Fe - sextet
	0.17	0.03	21.0	28.6	Fe_3C - sextet
	0.33	0.05	47.5	20.7	γ-Fe_2O_3 - sextet
	0.00	-	-	2.9	γ-Fe - singlet

Mössbauer spectra were measured at different temperatures, and they are presented in Fig. 1c and d (ferrofluid) and Fig. 2b (MWpyr WS:FF).

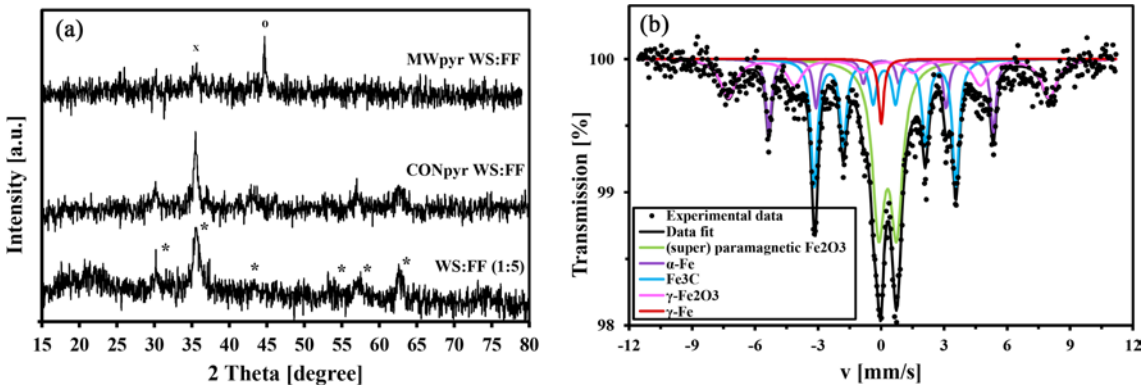

Fig. 2. X-ray powder diffraction analysis (a) of the initial sample (WS:FF) and synthetized magnetic biochars (MWpyr WS:FF; CONpyr WS:FF), as well as room temperature ^{57}Fe Mössbauer spectrum (b) of magnetic char after microwave pyrolysis (MWpyr WS:FF). Symbols: * = Maghemite; o = α-Fe or γ-Fe; x = non-stoichiometric Fe_3C.

According to Table 1, WS:FF contained 17.4% of iron (Fe_{total}) predominantly in the form of maghemite nanoparticles. The magnetic nanoparticles were responsible for the high value of volume magnetic susceptibility (493,150·10^{-6} SI units). After pyrolysis, the measured content of carbon decreased ($C^d_{CONpyr\ WS:FF}$=27.9%; $C^d_{MWpyr\ WS:FF}$=26.4%) and the total iron content of both samples increased differently ($Fe(total)_{CONpyr\ WS:FF}$ = 34.5%; $Fe(total)_{MWpyr\ WS:FF}$ = 40.4%). Despite the fact that iron content considerably increased, a loss of magnetic properties was recorded (Table 1). The measured value of the volume magnetic susceptibility decreased more than twice ($\kappa_{CONpyr\ WS:FF}$ = 185,515·10^{-6} SI units; $\kappa_{MWpyr\ WS:FF}$ = 188,995·10^{-6} SI units). Nevertheless, both samples are still strong magnetic materials, which enable them to be easily removed from water by applying a low-intensity magnetic field.

X-ray powder diffraction (Fig. 2a) was selected to find the main differences in phase distribution between both samples. It is clearly shown that the initial sample (composite of WS and FF) contained broad peaks assigned to magnetite/maghemite nanoparticles. In the case of conventional pyrolysis, the structure of magnetic particles was unchanged (the same diffraction pattern recorded in the sample before pyrolysis).

Microwave pyrolysis caused chemical changes of FFs. Only a few peaks were recorded by X-ray powder diffraction. Peaks of maghemite nanoparticles disappeared, and X-ray diffraction indicated that α-Fe, γ-Fe and Fe_3C could be generated. Consequently, for better identification of Fe-bearing components, ^{57}Fe Mössbauer spectroscopy was applied to describe iron phase transformation during the microwave pyrolysis (MWpyr WS:FF) (see Fig. 2b and Table 2). ^{57}Fe Mössbauer spectroscopy confirmed that maghemite nanoparticles presented in FFs reduce to metallic iron (14.3% of α-Fe and 2.9% of γ-Fe) and also react with carbon from biomass, and produced carbon iron (28.6% of Fe_3C) substances, probably with different stoichiometry. Moreover, iron oxide components (Fe_2O_3) are still present in the MWpyr WS:FF sample and show superparamagnetic behavior. Overall, it was shown that conventional pyrolysis performed at 550ºC is not able to cause phase changes in maghemite like in the case of microwave pyrolysis.

3.2. Textural properties and particle surface

Low-temperature nitrogen adsorption was used for characterization of textural properties of samples after the conventional and microwave pyrolysis. Both isotherms (Fig. 3a) were of type IV with a hysteresis loop corresponding with the capillary condensation in the mesopores [27].

The sample after microwave pyrolysis showed a higher volume of adsorbed gas in the whole range of relative pressure in comparison to the sample prepared by conventional method, which corresponds to the higher value of total pore volume and specific surface area, respectively (Table 3).

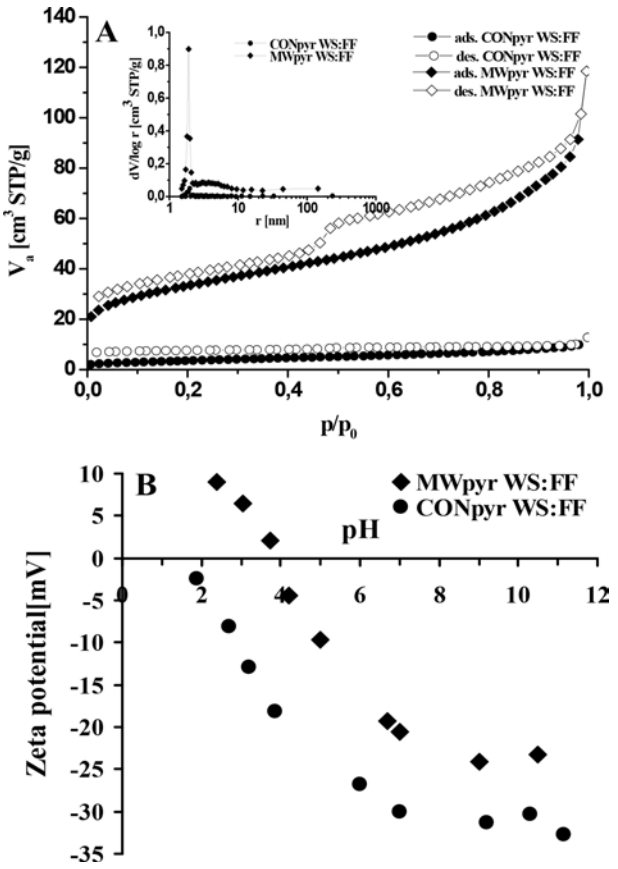

Fig. 3. Textural properties and pH dependent zeta potential of studied sorbents. (a) Adsorption and desorption isotherms of samples after conventional and microwave pyrolysis. Top left inset: pore size distribution curves of samples after conventional and microwave pyrolysis (STP means standard temperature and pressure, t=0°C, p=101.325 kPa). (b) Zeta potential of studied sorbents at different pH (pI (MWpyr WS:FF) = 4.0 and pI (CONpyr WS:FF) <1.9).

The hysteresis loop of both samples is open (decrease of desorbed gas volume is observed for relative pressure $p/p_0 \approx 0.45$). For CONpyr WS:FF, this could be caused by irreversible adsorption of molecules in pores with equal diameters as molecules of adsorbate. For the MWpyr WS:FF sample, this could also correspond to the higher microporosity [30]. While the value of micropore volume for the CONpyr WS:FF sample is under the interval of accuracy determination, for the MWpyr WS:FF sample the significant value of V_{micro} was obtained from the *t*-plot analysis. Also, the value of specific surface area is almost equal to the value of external surface for the CONpyr WS:FF sample. On the other hand, the value of external surface was lower than the specific surface of the MWpyr WS:FF sample, which also corresponds to the presence of micropores in its structure. From the shape of the pore size distribution curve for the CONpyr WS:FF sample, it can be concluded that the distribution is without the expressive maximum or broad distribution in the mesopore range, and the sample is meso-macroporous. The MWpyr WS:FF sample showed broader distribution in the range of pore diameters 4.5–16 nm (Fig. 3a, top left inset). In comparison to conventional pyrolysis, the microwave method allowed obtaining material with more developed porosity and texture, with a higher value of specific surface area, total pore volume and enhanced microporosity.

Except for the degree of porosity, distribution of micro/mesopores, sorption depends on the chemistry of the particle surface and electrochemical properties. However, both porosity and surface chemistry are related to each other. The zeta potential measurements (Fig. 3b) show that the IEP value of both samples is different. In comparison to MWpyr WS:FF, the sample after conventional pyrolysis shows a more negative value of zeta potential across the whole pH range. The sample after microwave pyrolysis shows pH_{IEP} around 4, whereas the conventionally pyrolyzed composite exhibits a more positive value (pH_{IEP} <1.9). The more positive zeta potential value of MWpyr WS:FF marks the sample for better adsorption of anions via electrostatic forces (e.g., more positive adsorbate surface and negative anions of arsenic).

Since the sample after microwave pyrolysis shows better textural properties, it is different from the point of view of phase composition, and we were aware that it showed much better sorption properties (see section 3.3. Sorption properties versus pH and adsorption isotherms). TEM and field emission scanning electron microscopy (FE-SEM) studies were also performed (Fig. 4). FE-SEM/energy dispersive X-ray analysis (EDX) confirmed a heterogeneous distribution of iron onto carbon matrix. EDX mapping (Fig. 4b) shows that some parts are completely coated with

Table 3. Textural parameters of samples after conventional and microwave pyrolysis

Sample	S_{BET} ($m^2\ g^{-1}$)	C_{BET}	V_{total} ($cm^3\ g^{-1}$)	V_{micro} ($cm^3\ g^{-1}$)	S_{ext} ($m^2\ g^{-1}$)
CONpyr WS:FF	13.0	71	0.0198	0.0002	12.4
MWpyr WS:FF	119.3	884	0.1832	0.0108	93.3

The values of specific surface area (S_{BET}), C_{BET} constant, total pore volume (V_{total}), volume of micropores and external surface (S_{ext}) calculated from the BET isotherm and *t*-plot method.

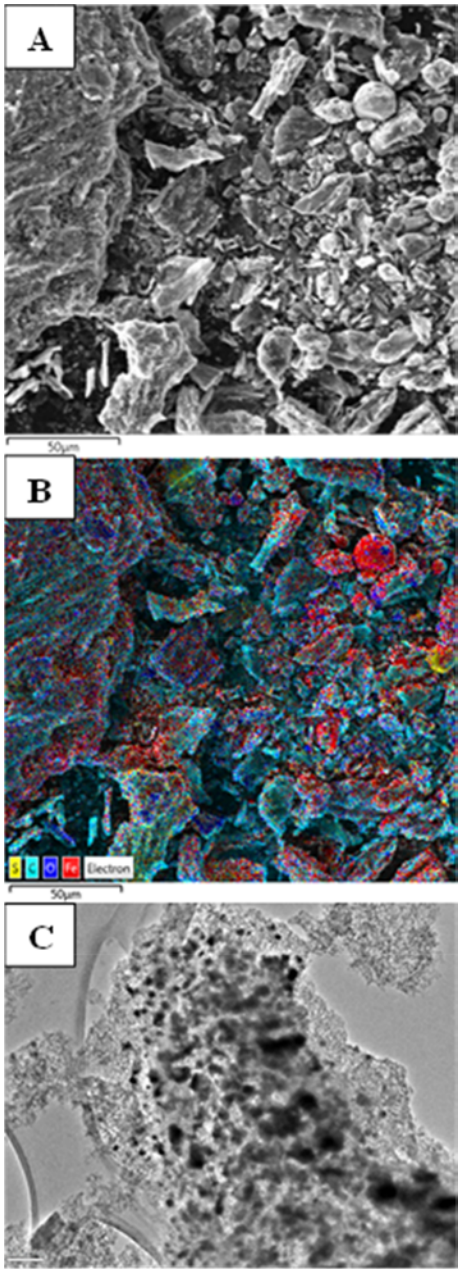

Fig. 4. Field emission scanning electron micrograph (a) with EDX analysis (b) and HR-TEM image (c) of the MWpyr WS:FF sample.

iron (red color). Fig. 4c shows a typical TEM image of the MWpyr WS:FF sample. The black particles with different size can be assigned to iron-based components, which are loaded on amorphous carbon biochar. The size of the iron -bearing particles is different (from several nanometers to 100 nm). The difference is caused by the process of agglomeration (particles of different size and shape are held together by weak physical interactions) and aggregation of the iron-based particles during the pyrolysis process. The heterogeneous particles are coupled to each other and/or they are incorporated into the carbon matrix derived from biomass. Note that the sample contains several iron-bearing components, as confirmed by X-ray powder diffraction and Mössbauer spectroscopy.

3.3. Sorption properties versus pH and adsorption isotherms

The sorption affinity of both samples (CONpyr WS:FF, MWpyr WS:FF) of As(V) and MB were investigated. Adsorption of As(V) and MB strongly depends on pH (Figs. 5a and 6a, respectively). As(V) present in the aqueous solution occurs in the form of oxyanions; MB is a cationic dye.

Compared to conventional pyrolysis, where the sorption of As(V) was relatively low across the whole pH range, the magnetic biochar coming from microwave pyrolysis showed excellent sorption properties (Fig. 5a). The best sorption was reached at acidic pH (45.4 mg of As per gram of MWpyr WS:FF). On the other hand, iron leaching from the magnetic biochar (MWpyr WS:FF) under pH 3.5 was observed (see Fig. 5a, top right inset). It proved that the sample after microwave pyrolysis is unstable in acidic conditions (pH <3.5), whereas the CONpyr WS:FF sample was unaffected from the point of view of iron leaching. The next goal was to determine the maximum sorption capacity of the adsorbent. Experiments based on the determination of maximum sorption capacity (Q_m) or adsorption isotherms were carried out at stable conditions (pH >3.5). Equilibrium pH 4 was selected to determine Q_m and the mechanism of the sorption process. Figure 5B shows experimental data of sorption capacity at different initial concentration of As(V) for the MWpyr WS:FF sample. The isotherms have been fitted according to the Langmuir and Freundlich models. In comparison to the Freundlich model (R^2=0.777), the adsorption process is better characterized by the Langmuir model with a correlation coefficient of R^2=0.998. The maximum sorption capacity calculated from the Langmuir isotherm (Eq. 3) was 25.6 mg g^{-1}. The high adsorption capacity was also confirmed by high value of the Freundlich constant (K_F = 7.87 L g^{-1}) calculated according to Eq. 4.

Additionally, both magnetic biochars were tested as a sorbents of cationic MB (Fig. 6a). Increased adsorption of MB due to increasing pH was observed. This is related to the electrostatic attraction between the positively charged adsorbate (MB) and the negatively charged adsorbent surface. The biggest jump in the sorption capacity value of both of the tested samples was observed from pH 9.9 to 10.9. The best adsorption was observed at pH 10.9, which corresponds with previously published papers [31,32]. The microwave pyrolyzed sample showed higher adsorption capacity compared to the sample prepared by the conventional method. Since there is a big increase of MB sorption between pH 9.9 and 10.9, the experiments related to maximum sorption capacity determination were performed at different pH values (Fig. 6b). The aim was to compare the adsorption mechanism. Freundlich and Langmuir models were applied for evaluation of adsorption isotherms at pH 7.0, 9.9 and 10.9. The highest maximum sorption capacity was obtained at pH 10.9 (Q_m = 144.9 mg g^{-1}). Then, with decreasing pH, the sorption affinity decreases (Q_m = 56.8 mg g^{-1} at pH 7). The Langmuir model appeared to

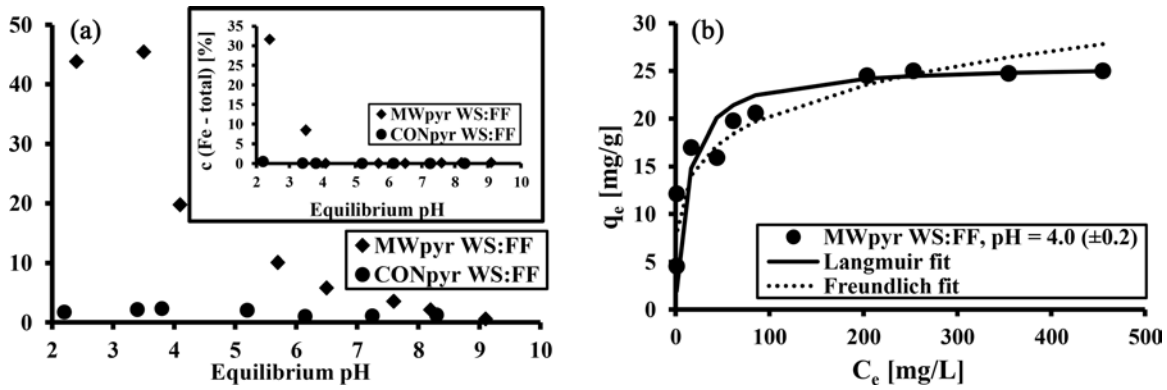

Fig. 5. Adsorption of arsenic (V) with magnetic biochars. (a) The sorption capacity of magnetic biochars of As(V) at different pH. Top right inset: Iron leaching after sorption of As(V) at different pH. Conditions: batch-type system; sorbent concentration 2 g L^{-1}; initial As(V) concentration 99.3 mg L^{-1}; room temperature. (b) Langmuir and Freundlich adsorption isotherms for As(V). Conditions: sample MWpyr WS:FF; batch-type system; sorbent concentration 2 g/L; initial metal concentration 10–500 mg L^{-1}; pH = 4.0±0.2; room temperature.

be the best method for fitting the adsorption isotherms at pH 7.0 and pH 9.9, respectively (see correlation coefficients in Table 4). An exception is at pH 10.9, where the isotherm can be fitted by both the Langmuir (R^2=0.981) and Freundlich models (R^2=0.947). This suggests that the mechanism of the adsorption process of MB is different as it was in the case of pH 7.0 or 9.9.

4. Discussions

4.1. Comments to the microwave pyrolysis

Initially, WS (without any susceptor) was pyrolyzed by microwaves; however, only water evaporated, and no other effect was observed (for example, carbonization, gas and oil production). In contrast, WS mixed with FF caused a strong exothermal process connected with liquefaction and gas production after one minute of microwave irradiation in briquette form. The magnetic nanoparticles inherited by FFs were a susceptor of microwaves during the pyrolysis. The microwave pyrolysis process of the sample can be described as follows. Microwaves penetrate the sample and continue to decay, and the microwave energy is transformed into heat. Microwave pyrolysis is carried out layer by layer, and thus from inside to outside [33]. Parts of the biomass particles are heated rapidly and decompose into carbon and volatiles. Since the pyrolysis of the internal material occurs first, the primary pyrolysis products released will pass through a low temperature zone and thus, the probability of occurrence of secondary cracking drops significantly. Due to the heat transfer, the external particles are heated and pyrolyzed again, and most of the volatiles released in the process are diffused to the low temperature area outside, while only a few are diffused to the internal high temperature zone [33]. During the microwave irradiation, the carbon plays the role of reducing agent. Inside the microwave-irradiated briquette, the heating and the reduction are taking place locally. Microwave-induced carbothermic reductions show that the reductions are occurring at temperatures lower than by conventional heating, the rates are faster and the form and quantity of the carbon employed plays an important role in the course of the reduction. Inside the microwave-irradiated composite, localized reduction microenvironments are generated [34]. In our case, indirect temperature measurement showed the maximum temperature on the surface to be 950°C. We assumed that a higher temperature was generated inside the sample, as red-hot points and in some cases white points were observed.

4.2. Discussion on phase analysis and physicochemical properties

Table 1 contains the general characterization (elemental [CHNS] analysis, ash content, total iron content and volume magnetic susceptibility) of the material before pyrolysis as well as after microwave conversion and conventional heating under nitrogen atmosphere. One notable result is that both pyrolyzed products still possess a high value of volume magnetic susceptibility, although volume magnetic susceptibility decreases by more than 50%. Surprisingly, at microwave irradiation where phase transformation of iron-bearing components was detected (see X-ray diffraction and Mössbauer spectroscopy) and high temperature was generated, the high magnetic susceptibility of the component was demonstrated. According to X-ray diffraction, conventional pyrolysis at 550°C has no effect on the iron oxide structure. The spinel structure is present in both spectra (before and after conventional conversion). Decreased volume magnetic susceptibility indicates the redistribution of Fe atoms in the spinel structure or maghemite phase degradation; however, it is difficult to recognize this by X-ray diffraction. In the case of microwave pyrolysis, iron oxide was reduced by pyrolyzed carbon according to the reaction:

$$Fe_3O_4 \rightarrow Fe_2O_3 \rightarrow FeO \rightarrow Fe \quad (5)$$

Products such as Fe_2O_3 and FeO, and final products such as α-Fe and γ-Fe can be formed in different stoichiometry. In this case, Mössbauer spectroscopy proved that microwave pyrolysis produces several phases such as Fe_3C (28.6%), (super) paramagnetic Fe_2O_3 (33.5%), α-Fe (14.3%), γ-Fe_2O_3 (20.7%) and γ-Fe (2.9%) (Table 2). As mentioned previously, during microwave

Table 4. Calculated values of Langmuir and Freundlich isotherm models

Sample description	Langmuir model			Freundlich model		
	Q_m (mg g^{-1})	b (L mg^{-1})	R^2	K_F (L g^{-1})	n	R^2
MWpyr WS:FF – As(V), pH=4.0	25.6	0.08224	0.998	7.87	4.85	0.777
MWpyr WS:FF – MB, pH=7.0	56.8	0.15398	0.994	18.5	4.56	0.695
MWpyr WS:FF – MB, pH=9.9	78.7	0.14564	0.990	29.3	5.63	0.687
MWpyr WS:FF – MB, pH=10.9	144.9	0.13093	0.981	48.7	4.77	0.947

conversion, the sample is heated from the inside to the outside, and thus the oxidation/reduction conditions are not the same across the whole sample. The existence of metallic iron resulted from the high temperature and the presence of the reduction atmosphere during pyrolysis. The formation of new substances (carbides) is related with the phenomena of microwave heating, where the pyrolysis process is very quick and high temperature is generated. Finally, high local temperature and no oxygen access are responsible for the formation of metallic iron and iron carbides. Thus, Fe and Fe_3C is an indicator of a reduction environment, whereas Fe_2O_3 indicates oxidation conditions. All identified phases of Fe-bearing products contributed to the magnetic properties and the resulting magnetic susceptibility reflects individual iron-bearing phases. The final volume magnetic susceptibility was $188{,}995 \cdot 10^{-6}$ SI units. In comparison to the sample before pyrolysis, it reflects about 40% of magnetic susceptibility (Table 1). We assume that the decreasing of magnetic susceptibility is caused by a transformation of maghemite nanoparticles to the above characterized products during microwave conversion. In more detail, γ-Fe_2O_3 has a spinel ferrite structure similar to magnetite and is ferrimagnetic; α-Fe is in a cubic planar centred lattice with ferromagnetic properties and γ-Fe has antiferromagnetic properties. Moreover, Fe_3C possess an orthorhombic structure with ferromagnetic properties. It is well known that iron carbides (Fe_3C, Fe_5C_2, Fe_7C_3) have a higher saturation magnetization than α-Fe_2O_3 [35-37]. However, the magnetic properties allow the resulting product to be magnetically separated after sorption.

4.3. Adsorption of arsenic (V) and MB with magnetic biochar

The structure, porosity and chemical composition have a significant effect on the adsorption properties of prepared materials. Both samples (MWpyr WS:FF; CONpyr WS:FF) were tested in respect to the As(V) anion and cationic MB. The adsorption ability of the adsorbents relates to the chemical composition, physicochemical, textural and electrochemical properties.

Our investigation showed that microwave pyrolysis and conventional pyrolysis produce totally different products. For instance, the specific surface area and total pore volume of MWpyr WS:FF was nine times higher in comparison to CONpyr WS:FF. Moreover, during microwave conversion, new inorganic phases were identified by X-ray (Fig. 2a) and Mössbauer spectroscopy (Fig. 2b, Table 2). Various iron phases (superparamagnetic Fe_2O_3, α-Fe, Fe_3C, γ-Fe_2O_3, γ-Fe) provide sorption sites for arsenic in aqueous solutions, and thus greatly improve the composite removal ability of arsenic. In this study, magnetic biochar after conventional pyrolysis shows the sorption capacity of As(V) under 5 mg g^{-1} (Fig. 5a), which is higher as published in the majority of papers. For example, in the case of As(V), Zhang et al. [38] reported that the Q_m of biochar/γ-Fe_2O_3 composite was 3.147 mg g^{-1}. In this paper [38], the authors compare the sorption properties of several iron oxides as well as iron composites of As(V): γ-Fe_2O_3, 4.643 mg g^{-1} [39]; hydrous iron oxide, 8.0 mg g^{-1} [40]; iron modified activated carbon, 1.92–6.57 [41]; magnetite–maghemite nanoparticles, 10.6 mg g^{-1} [42]; perlite/γ-Fe_2O_3 composite, 4.64 mg g^{-1} [43]; flowerlike γ-Fe_2O_3, 4.75 mg g^{-1}; α-Fe_2O_3, 5.31 mg g^{-1}; and Fe_3O_4, 4.65 mg g^{-1} and commercial α-Fe_2O_3, 4.6 mg g^{-1} [44]. Wang et al. [17] showed that magnetic biochar synthesized by pyrolyzing a mixture of naturally-occurring hematite mineral and pinewood biomass had a much greater ability in removing arsenic from an aqueous solution in comparison to the unmodified biochar. Additionally, magnetic char has stronger magnetic properties and can be easily isolated and removed employing external magnets. The Langmuir maximum sorption capacity of As for unmodified biochar shows a satisfactory 0.265 mg g^{-1} and 0.429 mg g^{-1} for hematite modified biochar, respectively. It also indicates that the hematite modification roughly doubled the As sorption ability of the biochar.

In the case of MWpyr WS:FF, the maximum sorption capacity of As(V) obtained from the Langmuir isotherm (Eq. 3) was 25.6 mg g^{-1} at pH 4.0 (Fig. 5b). A higher value sorption capacity can be reached at lower pH values (Fig. 5a). In general, when the pH in the solution decreased, the positive charge on the interface between the particles and the solution increased, and the positive charge appeared on the surface. The sorption capacity increased to 45.4 mg g^{-1} at an initial concentration of As(V) 99.3 mg L^{-1}. Unfortunately, the stability of sorbent decreases with higher acidity (leaching of iron). In the case of magnetic adsorbents, only several papers present a maximum sorption capacity higher than 20 mg g^{-1}. Shen et al. [45] demonstrated that the monolayer adsorption capacity of As(V) onto mesoporous carbon aerogel adsorbent was 56.2 mg g^{-1} at pH 7.0. In a review by Mehta et al. [46], different magnetic adsorbents were compared for the removal of diverse pollutants such as heavy metals, non-metals, dyes and organic pollutants from water. For As(V) removal, several magnetic adsorbents showed a high value of Q_m (e.g., multi-walled boron nitride nanotubes functionalized with Fe_3O_4 nanoparticles, 32.2 mg g^{-1} [47]; cetyltrimethylammonium bromide modified Fe_3O_4 particles, 23.07 mg g^{-1} [48]; ascorbic acid-coated Fe_3O_4 nanoparticles, 16.56 mg g^{-1} [49]; superparamagnetic ultra-

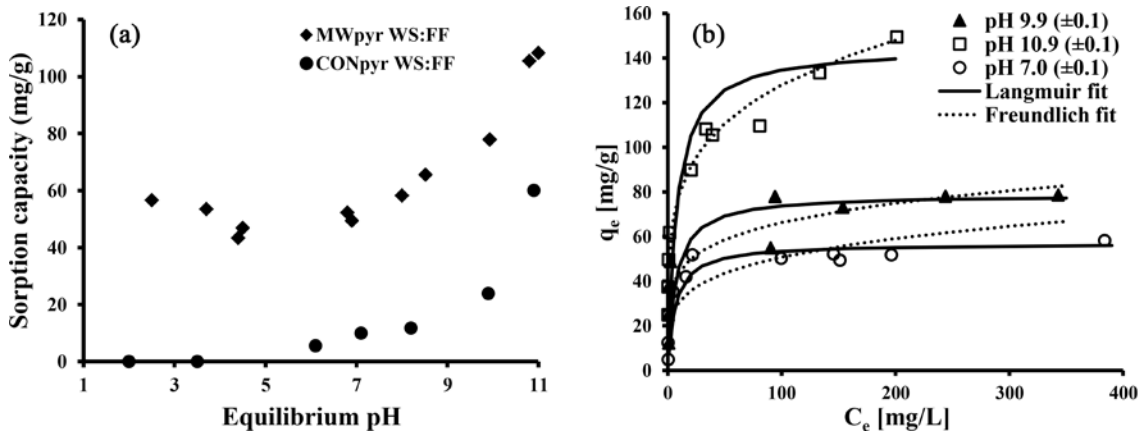

Fig. 6. Fig. 6. Adsorption of methylene blue with magnetic biochars. (a) The sorption capacity of magnetic biochars of MB at different pH. Conditions: batchtype system; sorbent concentration 2 g L^{-1}; initial MB concentration 250 mg L^{-1}; room temperature. (b) Langmuir and Freundlich adsorption isotherms for methylene blue adsorption at three different pH. Conditions: sample MWpyr WS:FF; batch-type system; sorbent concentration 2 g L^{-1}; initial MB concentration 10–500 mg L^{-1}; room temperature.

fine magnesium ferrite nanoparticles, 83.2 mg g^{-1} [50]; copper ferrite from PCB sludge, 45.66 mg g^{-1} [51]; and Fe_3O_4-loaded activated carbon from waste biomass, 204.2 mg g^{-1} [52]).

The positive effect of microwaves was proven also in the case of MB adsorption tests (Fig. 6a). Firstly, the conventionally pyrolyzed sample is inferior from the viewpoint of MB adsorption across the whole pH range compared to MWpyr WS:FF. The best adsorption properties of CONpyr WS:FF were observed in alkaline conditions at pH 10.9 (Q_e= 60 mg g^{-1}). A detailed analysis of MWpyr WS:FF by adsorption isotherms at three different pH values was carried out (Fig. 6b). The best sorption affinity was reached at pH 10.9 (Q_m=144.9 mg g^{-1}). The high adsorption capacity is caused by the combination of favorable properties of the sorbent (negative charge at alkaline pH, high specific surface area and porosity). Our results are comparable with the published data. For example, magnetic biochar derived from the empty fruit bunch showed a maximum adsorption capacity of 31.25 mg g^{-1} [14]. Thines et al. [53] studied the adsorption properties of MB on magnetic biochar. The maximum adsorption capacity of 87.32 mg g^{-1} at an optimum condition of pH 9 was found. A relatively high value of maximum sorption capacity of MB was reached by humic acid-coated Fe_3O_4 nanoparticles, 0.291 mmol g^{-1} [54]; magnetic chitosan/graphene oxide, 180.83 mg g^{-1} [55]; graphene nanosheet/magnetite composite, 43.82 mg g^{-1} [56]; Fe_3O_4 modified with 3-glycidoxypropyltrimethoxysilane and glycine, 158 mg g^{-1} [57]; carbon nanotube modified magnetic nanoparticles, 48.1 mg g^{-1} [58]; and epichlorohydrin -reticulated magnetic alginate beads, 0.7 mmol g^{-1} [59].

5. Conclusions

This study demonstrated that microwave pyrolysis is an economical and simple procedure for the synthesis of magnetic sorbents from agricultural waste biomass (WS) and FF. Magnetic biochar showed excellent sorption properties (Q_m(As)=25.6 mg g^{-1}; Q_m(MB)=144.9 mg g^{-1}). In comparison to conventional pyrolysis, one-step microwave conversion allowed obtaining material with different chemical composition (various Fe-bearing phases identified by Mössbauer spectroscopy, e.g., Fe_3C (28.6%), Fe_2O_3 (33.5%), α-Fe (14.3%), γ-Fe_2O_3 (20.7%), γ-Fe (2.9%)), more developed porosity and texture. Since the low-cost adsorbent showed a relatively high value of volume magnetic susceptibility, it can be easily removed from aqueous solution after sorption by magnetic separation.

Conflict of Interest

No potential conflict of interest relevant to this article was reported.

Acknowledgements

We are grateful to Dr. V. Girman for the HR-TEM studies. This work has been supported by the Slovak Grant Agency for Science VEGA (project No. 2/0158/15), the Marie Curie Programme FP7-People-2013-IAAP-WaSClean project No. 612250, as well as the Slovak R&D Agency project No. APVV-10-0252-WATRIP. This publication also results from the project implementation *Research excellence centre on earth sources, extraction and treatment* – 2nd phase (ITMS: 26220120038) and NanoCEXmat II (ITMS 26220120035), both supported by the Research & Development Operational Programme funded by the ERDF.

References

[1] Vaclavikova M, Gallios GP, Hredzak S, Jakabsky S. Removal of arsenic from water streams: an overview of available techniques. Clean Technol Environ Policy, 10, 89 (2008). https://doi.org/10.1007/s10098-007-0098-3.

[2] Zhang H, Shi H, Chen J, Zhao K, Wang L, Hao Y. Elemental mercury removal from syngas at high-temperature using activated char

pyrolyzed from biomass and lignite. Korean J Chem Eng, 33, 3134, (2016). https://doi.org/10.1007/s11814-016-0182-7.

[3] Bailey SE, Olin TJ, Bricka RM, Adrian DD. A review of potentially low-cost sorbents for heavy metals. Water Res, 33, 2469 (1999). https://doi.org/10.1016/S0043-1354(98)00475-8.

[4] Zubrik A, Matik M, Hredzák S, Lovás M, Danková Z, Kováčová M, Briančin J. Preparation of chemically activated carbon from waste biomass by single-stage and two-stage pyrolysis. J Cleaner Prod, 143, 643 (2017). https://doi.org/10.1016/j.jclepro.2016.12.061.

[5] Lee HW, Park RS, Park SH, Jung SC, Jeon JK, Kim SC, Chung JD, Choi WG, Park YK. Cu^{2+} ion reduction in wastewater over RDF-derived char. Carbon Lett, 18, 49 (2016). https://doi.org/10.5714/CL.2016.18.049.

[6] Lee H, Park RS, Lee HW, Hong Y, Lee Y, Park SH, Jung SC, Yoo KS, Jeon JK, Park YK. Adsorptive removal of atmospheric pollutants over Pyropia tenera chars. Carbon Lett, 19, 79 (2016). https://doi.org/10.5714/CL.2016.19.079.

[7] Magnacca G, Guerretta F, Vizintin A, Benzi P, Valsania MC, Nisticò R. Preparation, characterization and environmental/electrochemical energy storage testing of low-cost biochar from natural chitin obtained via pyrolysis at mild conditions. Appl Surf Sci, 427, 883 (2018). https://doi.org/10.1016/j.apsusc.2017.07.277.

[8] Cha JS, Park SH, Jung SC, Ryu C, Jeon JK, Shin MC, Park YK. Production and utilization of biochar: a review. J Ind Eng Chem, 40, 1 (2016). https://doi.org/10.1016/j.jiec.2016.06.002.

[9] Ahmadi M, Kouhgardi E, Ramavandi B. Physico-chemical study of dew melon peel biochar for chromium attenuation from simulated and actual wastewaters. Korean J Chem Eng, 33, 2589 (2016). https://doi.org/10.1007/s11814-016-0135-1.

[10] Li G, Zhu W, Zhu L, Chai X. Effect of pyrolytic temperature on the adsorptive removal of p-benzoquinone, tetracycline, and polyvinyl alcohol by the biochars from sugarcane bagasse. Korean J Chem Eng, 33, 2215 (2016). https://doi.org/10.1007/s11814-016-0067-9.

[11] Park SH, Cho HJ, Ryu C, Park YK. Removal of copper(II) in aqueous solution using pyrolytic biochars derived from red macroalga Porphyra tenera. J Ind Eng Chem, 36, 314 (2016). https://doi.org/10.1016/j.jiec.2016.02.021.

[12] Zhu J, Yu JX, Chen JD, Zhang JS, Tang JQ, Xu YL, Zhang YF, Chi RA. Effects of co-ion initial concentration ratio on removal of Pb^{2+} from aqueous solution by modified sugarcane bagasse. Korean J Chem Eng, 34, 1721 (2017). https://doi.org/10.1007/s11814-017-0061-x.

[13] Spokas KA, Koskinen WC, Baker JM, Reicosky DC. Impacts of woodchip biochar additions on greenhouse gas production and sorption/degradation of two herbicides in a Minnesota soil. Chemosphere, 77, 574 (2009). https://doi.org/10.1016/j.chemosphere.2009.06.053.

[14] Fathy NA, Girgis BS, Khalil LB, Farah JY. Utilization of cotton stalks-biomass waste in the production of carbon adsorbents by KOH activation for removal of dye-contaminated water. Carbon Lett, 11, 224 (2010). https://doi.org/10.5714/cl.2010.11.3.224.

[15] Gallios GP, Vaclavikova M. Removal of chromium (VI) from water streams: a thermodynamic study. Environ Chem Lett, 6, 235 (2008). https://doi.org/10.1007/s10311-007-0128-8.

[16] Zhang G, Qu J, Liu H, Cooper AT, Wu R. $CuFe_2O_4$/activated carbon composite: a novel magnetic adsorbent for the removal of acid orange II and catalytic regeneration. Chemosphere, 68, 1058 (2007). https://doi.org/10.1016/j.chemosphere.2007.01.081.

[17] Wang S, Gao B, Zimmerman AR, Li Y, Ma L, Harris WG, Migliaccio KW. Removal of arsenic by magnetic biochar prepared from pinewood and natural hematite. Bioresour Technol, 175, 391 (2015). https://doi.org/10.1016/j.biortech.2014.10.104.

[18] Thines KR, Abdullah EC, Mubarak NM, Ruthiraan M. Synthesis of magnetic biochar from agricultural waste biomass to enhancing route for waste water and polymer application: a review. Renewable Sustainable Energy Rev, 67, 257 (2017). https://doi.org/10.1016/j.rser.2016.09.057.

[19] Safarik I, Horska K, Pospiskova K, Filip J, Safarikova M. Mechanochemical synthesis of magnetically responsive materials from non-magnetic precursors. Mater Lett, 126, 202 (2014). https://doi.org/10.1016/j.matlet.2014.04.045.

[20] Mubarak NM, Fo YT, Al-Salim HS, Sahu JN, Abdullah EC, Nizamuddin S, Jayakumar NS, Ganesan P. Removal of methylene blue and orange-G from waste water using magnetic biochar. Int J Nanosci, 14, 1550009 (2015). https://doi.org/10.1142/S0219581X1550009X.

[21] Jiang X, Shen D. Pb(II) ion adsorption by biomass-based carbonaceous fiber modified by the integrated oxidation and vulcanization. Korean J Chem Eng, 34, 2619 (2017). https://doi.org/10.1007/s11814-017-0162-6.

[22] Lovás M, Znamenáčková I, Zubrik A, Kováčová M, Dolinská S. The application of microwave energy in mineral processing: a review. Acta Montan Slovaca, 16, 137 (2011).

[23] Salema AA, Ani FN. Microwave-assisted pyrolysis of oil palm shell biomass using an overhead stirrer. J Anal Appl Pyrolysis, 96, 162 (2012). https://doi.org/10.1016/j.jaap.2012.03.018.

[24] Zuo W, Tian Y, Ren N. The important role of microwave receptors in bio-fuel production by microwave-induced pyrolysis of sewage sludge. Waste Manage, 31, 1321 (2011). https://doi.org/10.1016/j.wasman.2011.02.001.

[25] Jakabský Š, Zaťko S, Bakoš J, Zálešáková E. Preparation of ferrofluid. Czechoslovak Patent No. 223,697 (1982).

[26] Brunauer S, Emmett PH, Teller E. Adsorption of gases in multimolecular layers. J Am Chem Soc, 60, 309 (1938). https://doi.org/10.1021/ja01269a023.

[27] Rouquerol J, Avnir D, Fairbridge CW, Everett DH, Haynes JM, Pernicone N, Ramsay JDF, Sing KSW, Unger KK. Recommendations for the characterization of porous solids (technical report). Pure Appl Chem, 66, 1739 (1994). https://doi.org/10.1351/pac199466081739.

[28] Langmuir I. The constitution and fundamental properties of solids and liquids. Part I. solids. J Am Chem Soc, 38, 2221 (1916). https://doi.org/10.1021/ja02268a002.

[29] Freundlich H. Über die Adsorption in Lösungen. Zeitschrift für Physikalische Chemie, 57, 385 (1906). https://doi.org/10.1515/zpch-1907-5723.

[30] Hudec P. Texture of Solids–Determination of Surface Properties of Adsorbents and Catalysts by Physical Adsorption of Nitrogen (In Slovak), Slovak Technical University Publisher, Bratislava (2012).

[31] Kumar A, Jena HM. Removal of methylene blue and phenol onto prepared activated carbon from Fox nutshell by chemical activation in batch and fixed-bed column. J Cleaner Prod, 137, 1246 (2016). https://doi.org/10.1016/j.jclepro.2016.07.177.

[32] Bulut Y, Aydın H. A kinetics and thermodynamics study of methylene blue adsorption on wheat shells. Desalination, 194, 259 (2006). https://doi.org/10.1016/j.desal.2005.10.032.

[33] Zhao X, Wang W, Liu H, Ma C, Song Z. Microwave pyrolysis of wheat straw: product distribution and generation mechanism.

Bioresour Technol, 158, 278 (2014). https://doi.org/10.1016/j.biortech.2014.01.094.

[34] Ishizaki K, Nagata K, Hayashi T. Localized heating and reduction of magnetite ore with coal in composite pellets using microwave irradiation. ISIJ Int, 47, 817 (2007). https://doi.org/10.2355/isijinternational.47.817.

[35] David B, Zboril R, Mashlan M, Grygar T, Dumitrache F, Schneeweiss O. Single ferromagnetic behaviour of nanopowders with Fe_3C. J Magn Magn Mater, 304, e787 (2006). https://doi.org/10.1016/j.jmmm.2006.02.224.

[36] Hofer LJE, Cohn EM. Saturation magnetizations of iron carbides. J Am Chem Soc, 81, 1576 (1959). https://doi.org/10.1021/ja01516a016.

[37] Dong XL, Zhang ZD, Xiao QF, Zhao XG, Chuang YC, Jin SR, Sun WM, Li ZJ, Zheng ZX, Yang H. Characterization of ultrafine γ-Fe(C), α-Fe(C) and Fe3C particles synthesized by arc-discharge in methane. J Mater Sci, 33, 1915 (1998). https://doi.org/10.1023/A:1004369708540.

[38] Zhang M, Gao B, Varnoosfaderani S, Hebard A, Yao Y, Inyang M. Preparation and characterization of a novel magnetic biochar for arsenic removal. Bioresour Technol, 130, 457 (2013). https://doi.org/10.1016/j.biortech.2012.11.132.

[39] Park H, Myung NV, Jung H, Choi H. As(V) remediation using electrochemically synthesized maghemite nanoparticles. J Nanopart Res, 11, 1981 (2009). https://doi.org/10.1007/s11051-008-9558-x.

[40] Xue Y, Gao B, Yao Y, Inyang M, Zhang M, Zimmerman AR, Ro KS. Hydrogen peroxide modification enhances the ability of biochar (hydrochar) produced from hydrothermal carbonization of peanut hull to remove aqueous heavy metals: Batch and column tests. Chem Eng J, 200-202, 673 (2012). https://doi.org/10.1016/j.cej.2012.06.116.

[41] Gu Z, Fang J, Deng B. Preparation and evaluation of GAC-based iron-containing adsorbents for arsenic removal. Environ Sci Technol, 39, 3833 (2005). https://doi.org/10.1021/es048179r.

[42] Chowdhury SR, Yanful EK. Arsenic and chromium removal by mixed magnetite–maghemite nanoparticles and the effect of phosphate on removal. J Environ Manage, 91, 2238 (2010). https://doi.org/10.1016/j.jenvman.2010.06.003.

[43] Nguyen Thanh D, Singh M, Ulbrich P, Strnadova N, Štěpánek F. Perlite incorporating γ-Fe_2O_3 and α-MnO_2 nanomaterials: Preparation and evaluation of a new adsorbent for As(V) removal. Sep Purif Technol, 82, 93 (2011). https://doi.org/10.1016/j.seppur.2011.08.030.

[44] Zhong LS, Hu JS, Liang HP, Cao AM, Song WG, Wan LJ. Self-assembled 3D flowerlike iron oxide nanostructures and their application in water treatment. Adv Mater, 18, 2426 (2006). https://doi.org/10.1002/adma.200600504.

[45] Shen G, Xu Y, Liu B. Preparation and adsorption properties of magnetic mesoporous Fe_3C/carbon aerogel for arsenic removal from water. Desalin Water Treat, 57, 24467 (2016). https://doi.org/10.1080/19443994.2016.1138895.

[46] Mehta D, Mazumdar S, Singh SK. Magnetic adsorbents for the treatment of water/wastewater: a review. J Water Process Eng, 7, 244 (2015). https://doi.org/10.1016/j.jwpe.2015.07.001.

[47] Chen R, Zhi C, Yang H, Bando Y, Zhang Z, Sugiur N, Golberg D. Arsenic (V) adsorption on Fe_3O_4 nanoparticle-coated boron nitride nanotubes. J Colloid Interface Sci, 359, 261 (2011). https://doi.org/10.1016/j.jcis.2011.02.071.

[48] Jin Y, Liu F, Tong M, Hou Y. Removal of arsenate by cetyltrimethylammonium bromide modified magnetic nanoparticles. J Hazard Mater, 227-228, 461 (2012). https://doi.org/10.1016/j.jhazmat.2012.05.004.

[49] Feng L, Cao M, Ma X, Zhu Y, Hu C. Superparamagnetic high-surface-area Fe3O4 nanoparticles as adsorbents for arsenic removal. J Hazard Mater, 217-218, 439 (2012). https://doi.org/10.1016/j.jhazmat.2012.03.073.

[50] Tang W, Su Y, Li Q, Gao S, Shang JK. Superparamagnetic magnesium ferrite nanoadsorbent for effective arsenic (III, V) removal and easy magnetic separation. Water Res, 47, 3624 (2013). https://doi.org/10.1016/j.watres.2013.04.023.

[51] Tu YJ, You CF, Chang CK, Wang SL, Chan TS. Arsenate adsorption from water using a novel fabricated copper ferrite. Chem Eng J, 198-199, 440 (2012). https://doi.org/10.1016/j.cej.2012.06.006.

[52] Liu Z, Zhang FS, Sasai R. Arsenate removal from water using Fe_3O_4-loaded activated carbon prepared from waste biomass. Chem Eng J, 160, 57 (2010). https://doi.org/10.1016/j.cej.2010.03.003.

[53] Thines KR, Abdullah EC, Ruthiraan M, Mubarak NM. Production of magnetic biochar derived from durian's rind at vacuum condition for removal of methylene blue pigments from aqueous solution. Int J Chem Eng, 2, 13 (2015).

[54] Zhang X, Zhang P, Wu Z, Zhang L, Zeng G, Zhou C. Adsorption of methylene blue onto humic acid-coated Fe_3O_4 nanoparticles. Colloids Surf A Physicochem Eng Aspects, 435, 85 (2013). https://doi.org/10.1016/j.colsurfa.2012.12.056.

[55] Fan L, Luo C, Sun M, Li X, Lu F, Qiu H. Preparation of novel magnetic chitosan/graphene oxide composite as effective adsorbents toward methylene blue. Bioresour Technol, 114, 703 (2012). https://doi.org/10.1016/j.biortech.2012.02.067.

[56] Ai L, Zhang C, Chen Z. Removal of methylene blue from aqueous solution by a solvothermal-synthesized graphene/magnetite composite. J Hazard Mater, 192, 1515 (2011). https://doi.org/10.1016/j.jhazmat.2011.06.068.

[57] Zhang YR, Wang SQ, Shen SL, Zhao BX. A novel water treatment magnetic nanomaterial for removal of anionic and cationic dyes under severe condition. Chem Eng J, 233, 258 (2013). https://doi.org/10.1016/j.cej.2013.07.009.

[58] Madrakian T, Afkhami A, Ahmadi M, Bagheri H. Removal of some cationic dyes from aqueous solutions using magnetic-modified multi-walled carbon nanotubes. J Hazard Mater, 196, 109 (2011). https://doi.org/10.1016/j.jhazmat.2011.08.078.

[59] Rocher V, Bee A, Siaugue JM, Cabuil V. Dye removal from aqueous solution by magnetic alginate beads crosslinked with epichlorohydrin. J Hazard Mater, 178, 434 (2010). https://doi.org/10.1016/j.jhazmat.2010.01.100.